The International Journal of Advanced Manufacturing Technology (2023) 127:3255–3267
https://doi.org/10.1007/s00170-023-11250-2

ORIGINAL ARTICLE

Mechanical and microstructural characterization of aluminium micro-pins realized by cold metal transfer

Christian Schneider-Bröskamp[1] · Martin Schnall[1] · Alois Birgmann[1] · Stephan Ucsnik[1]

Received: 25 November 2022 / Accepted: 8 March 2023 / Published online: 12 June 2023

Abstract

The European collaborative research project ADALFIC (Advanced Aluminium Fittings in CFRP tubes) focuses on the design, analysis, manufacturing and testing of ultra-lightweight carbon fiber reinforced plastic (CFRP) tubes with integrated aluminium end fittings. Reliable joining technologies for combining aluminium and CFRP are of great interest since the combination of superior mechanical properties and low density offer a wide range of applications. One such approach is the use of form locking micro-pins on the surface of the metallic part enabling the joint between metal and CFRP by mechanical interlocking. In this work Fronius' Cold-Metal-Transfer (CMT) Print welding technology was used to generate very small, minimum-mass, spike-head pins, which are optimized for form-locked joints between aluminium and CFRP components. The aluminium pins are characterized on a macroscopic and microscopic level using light optical microscopy and hardness testing. To evaluate the behavior of the pins under mode II load conditions a new shear testing method for pins was developed and implemented. With this test equipment the maximum shear force and ultimate shear strength of individual pins were measured at different temperatures and heat treatment conditions. The failure modes and fracture surfaces were analyzed via scanning electron microscopy. The results demonstrate that the *novel* spike-head CMT aluminium pins can withstand considerable shear forces, especially in the peak aged condition. This makes them a viable, flexible and lightweight option for form-locked aluminium-CFRP joints.

Keywords z-pins · Aluminium · Hybrid-joint · CMT

1 Introduction

The benefit of employing cold metal transfer (CMT) welded metallic pins as through thickness reinforcements in joints for metal sheets and fiber reinforced plastics is well documented in literature [1–6] and also used in the patent of Teufelberger [7] registered under the trademark of T-IGEL^{TM} joint technology. Most studies focus on the effects of pin reinforcement on the overall joint properties [1–6, 8–11] while only limited research was conducted, and is available on the performance and characteristics of the (single) pins themselves [12–15], as is the case in this work. Moreover, the majority of research was conducted on (stainless) steel, in some cases titanium pins [1, 3–5, 8, 9, 14], but only few results on aluminium pins are available [4, 6, 12].

Reisgen et al. [14] investigated the metallographic and mechanical properties of ER308LSi pins on AISI 304 sheets. They identified six different zones in the pin microstructure, which can be related to the different stages of the pin welding process and its associated solidification and reheating (T-gradient) history. Tensile testing revealed ductile fracture behavior of the pins, slightly depending on the overall heat input during *pinning*.

A systematic study on the influence of various welding parameters on the pin geometry on aluminium pins (AlSi5) was conducted by Zhang et al. [15]. Key parameters affecting the size and shape of the pins are: *bowlmelt* current, deposit velocity and cooldown time of the droplet. Similar, albeit less

✉ Christian Schneider-Bröskamp
christian.schneider-broeskamp@ait.ac.at

Martin Schnall
martin.schnall@ait.ac.at

Alois Birgmann
alois.birgmann@ait.ac.at

Stephan Ucsnik
stephan.ucsnik@ait.ac.at

[1] LKR Light Metals Technologies, Austrian Intitute of Technology (AIT), Lamprechtshausenerstraße 61, Braunau am Inn - Ranshofen 5282, Upper Austria, Austria

detailed, observations for steel pins (G3Si1) were made by Somosköi and Bianchi in [13, 16].

Four major different pin head shapes are reported in literature: cylindrical, ball head, spike, as well as ballhead-spike like pins [1, 2, 17]. The pin head geometry of latter two types influence the failure mode of composite joints. Cylindrical and spike pins promote pull-out failure, whereas ball head and ball head spike pins are more likely to fail in shear mode, since they offer increased resistance against being withdrawn from the composite [1].

The CMT pin welding process offers some flexibility in terms of pin height, reported pin heights in the literature range from 2.5 mm to 15 mm [4, 8, 9, 17]. Figure 1 shows the evolution of aluminium pins manufactured at LKR since 2010 starting with very tall Al-pins in 2010 (a) and constantly decreasing heights and improving pin-shapes by advanced process control (b), optimization of process parameters (c), or the use of local energy input d). In this study the minimum pin height was further decreased to 1.50 mm (Fig. 1 d) increasing the efficiency for ultra-lightweight design.

Table 1 Chemical composition (wt %) of the S AL 2319 filler metal and 2024 sheet material used in the welding experiments

	Si	Fe	Cu	Mn	Mg	Ti	Al
2319 wire	0.11	0.15	5.88	0.29	0.01	0.12	bal.
2024 sheet	0.21	0.31	4.39	0.79	1.55	0.065	bal.

While the fabrication and modification of aluminium pins is well understood as highlighted above, the mechanical performance of individual pins is poorly investigated. Numerous studies investigated the overall performance of *pin-enhanced* CFRP-metal joints consisting of a multitude of metallic pins thus only providing the cumulative strength of the pin array

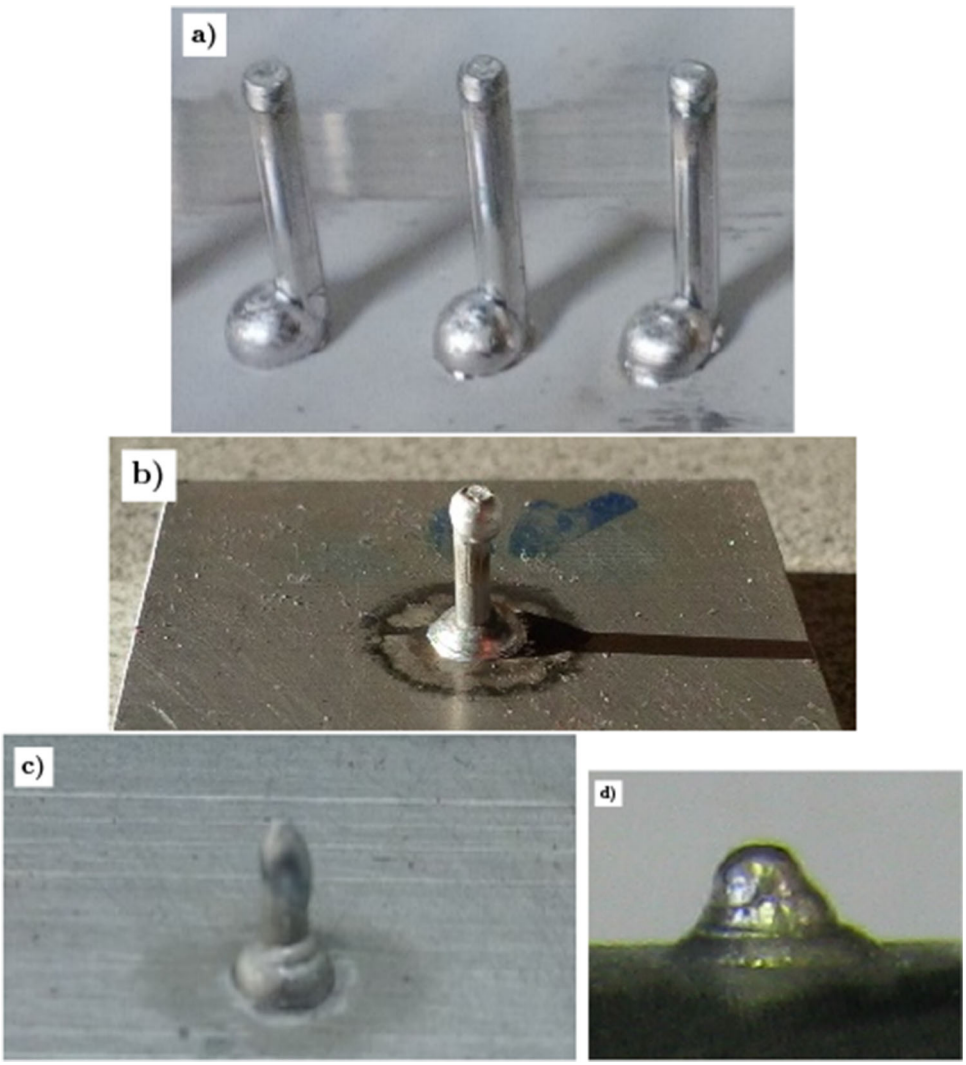

Fig. 1 Evolution of aluminium pins generated by CMT in the last 10 years: **a** cylinder pins AlSi5 (h=15 mm; project JOIN4+), **b** AlMgSc-pin (h=7.45 mm, project IWB-TB), **c** AlSi5-pin (h=4.2 mm, project IWB-TB), **d** S AL 2319 pin (h=1.50 mm, project ADALFIC & SUSTAINair). Pictures by courtesy of LKR Light Metals Technologies

Table 2 Mechanical properties of the S AL 2319 all weld metal in as-built condition and EN-AW 2024 sheet material in T351 condition

	Yield Strength MPa	Tensile Strength MPa	Elongation %
2319 wire	70	160	12
2024 sheet	397–412	552–556	12.4–15.2

[1–6, 8–11]. To the authors knowledge only Ucsnik et al. [6] conducted shear testing of individual aluminium pins demonstrating their suitability for ultra-lightweight CFRP-metal struts in aerospace applications. This work extends aforementioned results to different test temperatures and heat treatment conditions of the pins. Furthermore, additional metallographic characterization, hardness testing as well as fracture surface analysis was performed.

2 Experiments

2.1 Materials

EN-AW2024-T3 sheet material, 1 mm thick, was used as base plates in the welding experiments. S Al 2319 solid wire with a diameter of 1.2 mm was used as filler metal. The chemical composition and mechanical properties of the filler material are listed in Tables 1 and 2.

2.2 Welding

Instead of the *conventional* CMT Pin process, an adaption of Fronius' CMT Print technology (Fronius CMT Advanced 4000R + VR 7000-CMT 4R/G/W/F++, ABB IRB 4600-45/2.05 IRC5 robot equipped with a tilting rotary table) was used to achieve pin heights with an average of 1.50 mm. The precise control and timing of wire-feed, current and voltage allow the deposition of individual drops on the specimen. The size of the droplets and the weld pool on the surface can be modified via precise parameter variation.

The schematic in Fig. 2 shows the time-dependent wire-feed, current and voltage characteristics for the deposition of one drop in the CMT Print process. At the beginning of the process (1) the wire-feed is slowly ramped up while the voltage remains unchanged, and the current is very low. As soon as the wire touches the surface (2), a short circuit is completed resulting in a short circuit current and no-load voltage. At that moment the welding arc is sparked (3) by the short circuit current and the wire-feed is reversed while the voltage rises again. The electric arc melts the specimen surface and the tip of the welding wire. A droplet grows (4) at the tip and the wire tip is dipped into the weld pool (5).

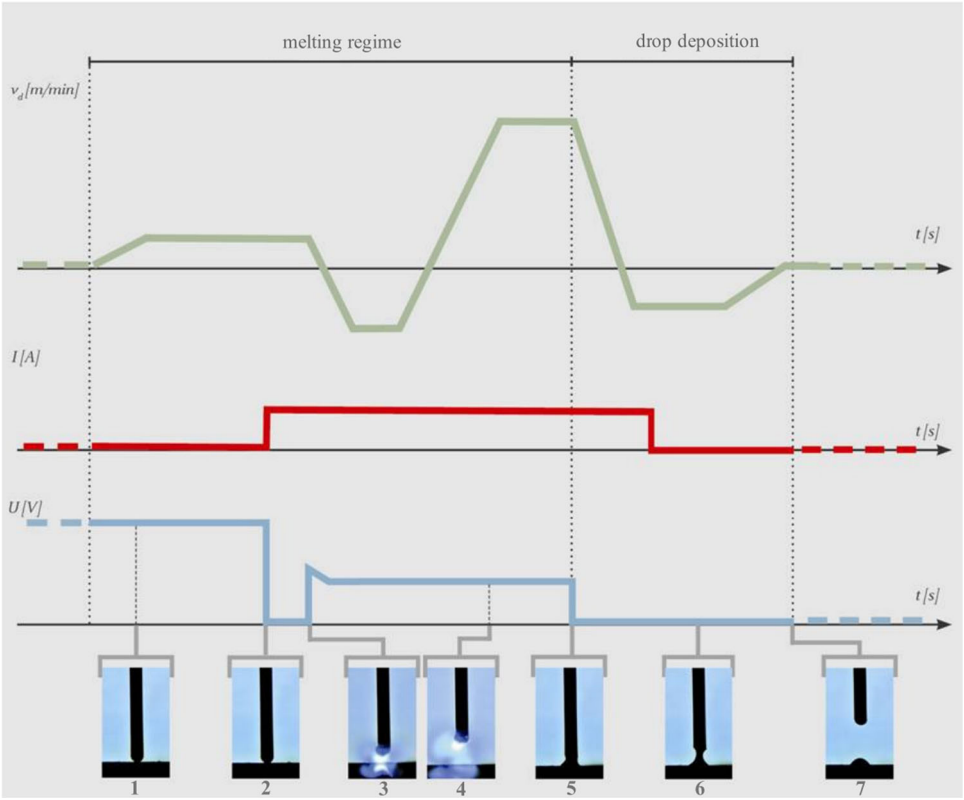

Fig. 2 Schematic, time-dependent wire-feed (v_d), current (I) and voltage (U) characteristics including corresponding high speed recordings of the pin process, modified from [18]

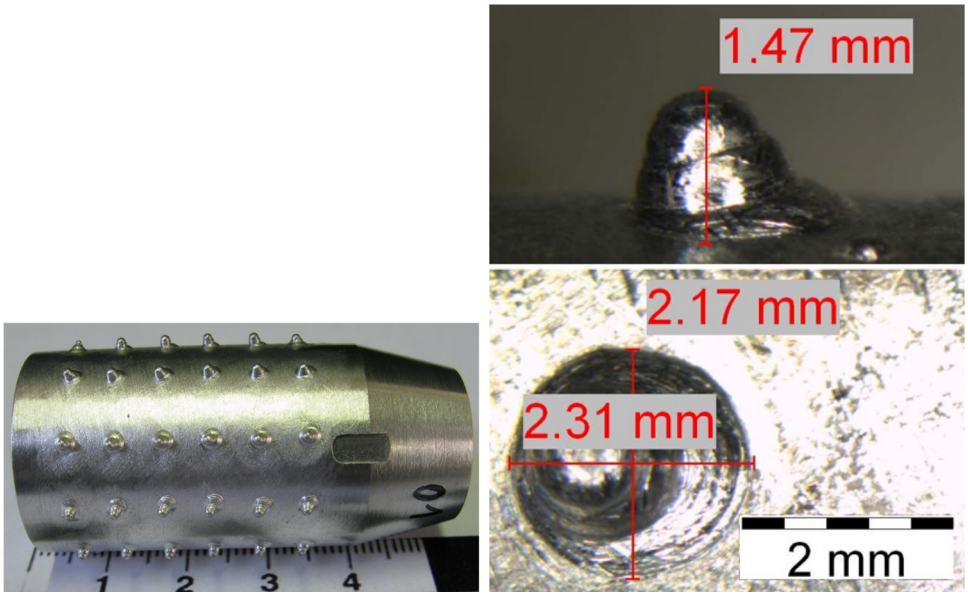

Fig. 3 AW2024 sleeve with S Al 2319 pins (left) and single pin dimensions height, d_{length}, d_{across} (right)

After the deposition the wire is retracted (6), and the process starts again or ends (7).

Three droplets with varying parameter settings are stacked on top of each other using the modified CMT Print mode to generate the new *spiky design* aluminium pins. Precise control of the parameters and boundary conditions is necessary to ensure a stable process and consistent deposition of pins. The cycle time for one pin is approximately 150 ms.

Figure 3 shows an exemplary row of S Al 2319 pins printed on an EN-AW2024 sleeve (left) together with the dimensions of one spiky pin in height-, d_{length}, and d_{across} direction.

2.3 Heat treatment

In general, the 2xxx class aluminium alloys retain their maximum strength only after appropriate heat treatment. In this case the peak aged condition (T6) was investigated in addition to the as-built condition to assess their influence on microstructure as well as mechanical properties in final pins.

The plates and pins were heated to 535°C for 90 min for solution annealing (Nabertherm furnace), water quenched and subsequently artificially aged at 175°C for 3 h (Heraeus furnace).

2.4 Shear testing

To test individual pins in the most prominent loading direction, namely the In-plane shear (mode II) direction, a special pin-coupon adapter for a standard tensile testing machine (Zwick Z100) was constructed and implemented (see Fig. 4). This adapter consists of three parts: a retainer with a V-shaped opening for the drawbar (1), a drawbar with a circular opening for the pins (2), and the specimen mount with a housing for the individual test plates (3).

During testing the sample plates (30x30x1 mm) are inserted in the specimen holder, which is then mounted onto

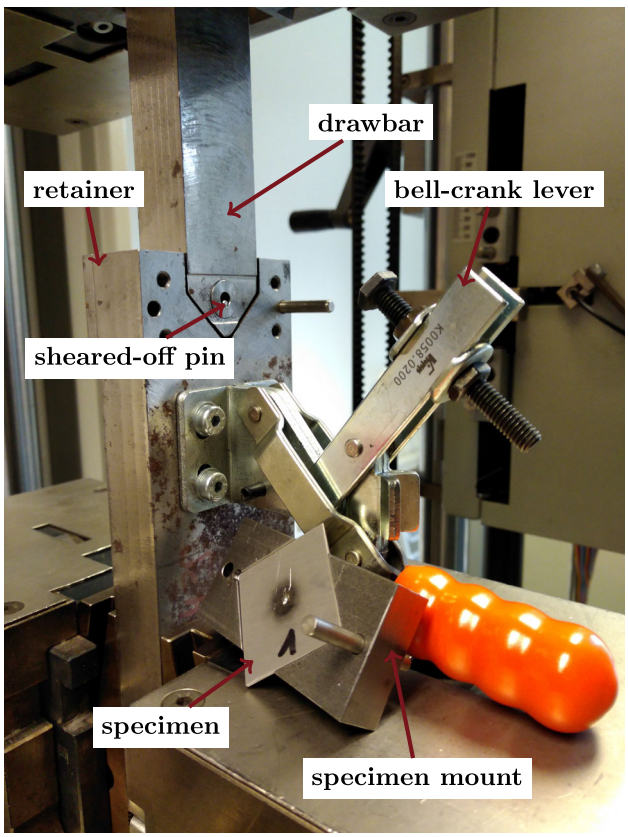

Fig. 4 Adapter on the tensile testing machine for mode II shear testing of individual pins

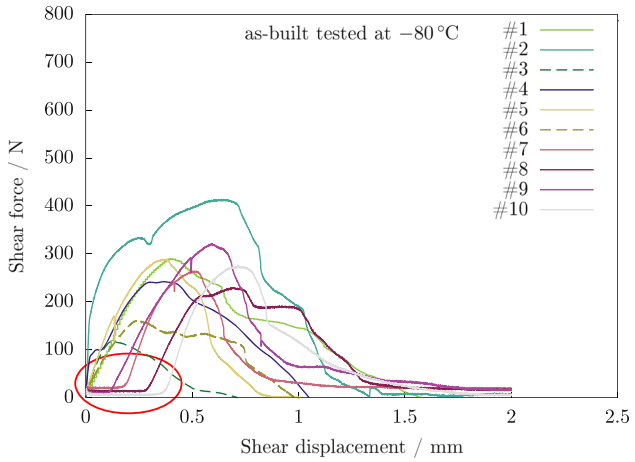

Fig. 5 Exemplary force-displacement curves of pin testing at -80°C Celsius showing staggering of the individual curves

the retainer by two high-precision bolts and additionally fixed with a fast-fixation bell-crank lever.

The drawbar is retracted and shears off the pins. Traverse resolution is used to record the shear displacement. The test speed was set to 1 mm min^{-1} and the maximum test distance limited to 2 mm. The pins are preloaded between 0 N to 100 N, depending on the test temperature of the coupons. The different preloading levels do not influence the maximum force recorded, which is the primary focus of the shear testing.

The shear tests revealed difficulties in the early stages of the experiment. The combination of global displacement measurement and settling effects of the specimens in the mount and the circular counterpart sometimes resulted in staggered force-displacement curves (see Fig. 5). These effects could potentially be eliminated by a local displacement measurement during testing, which will be implemented for future investigations. However, this shift does not influence the maximum force recorded and the overall quality of the measurement.

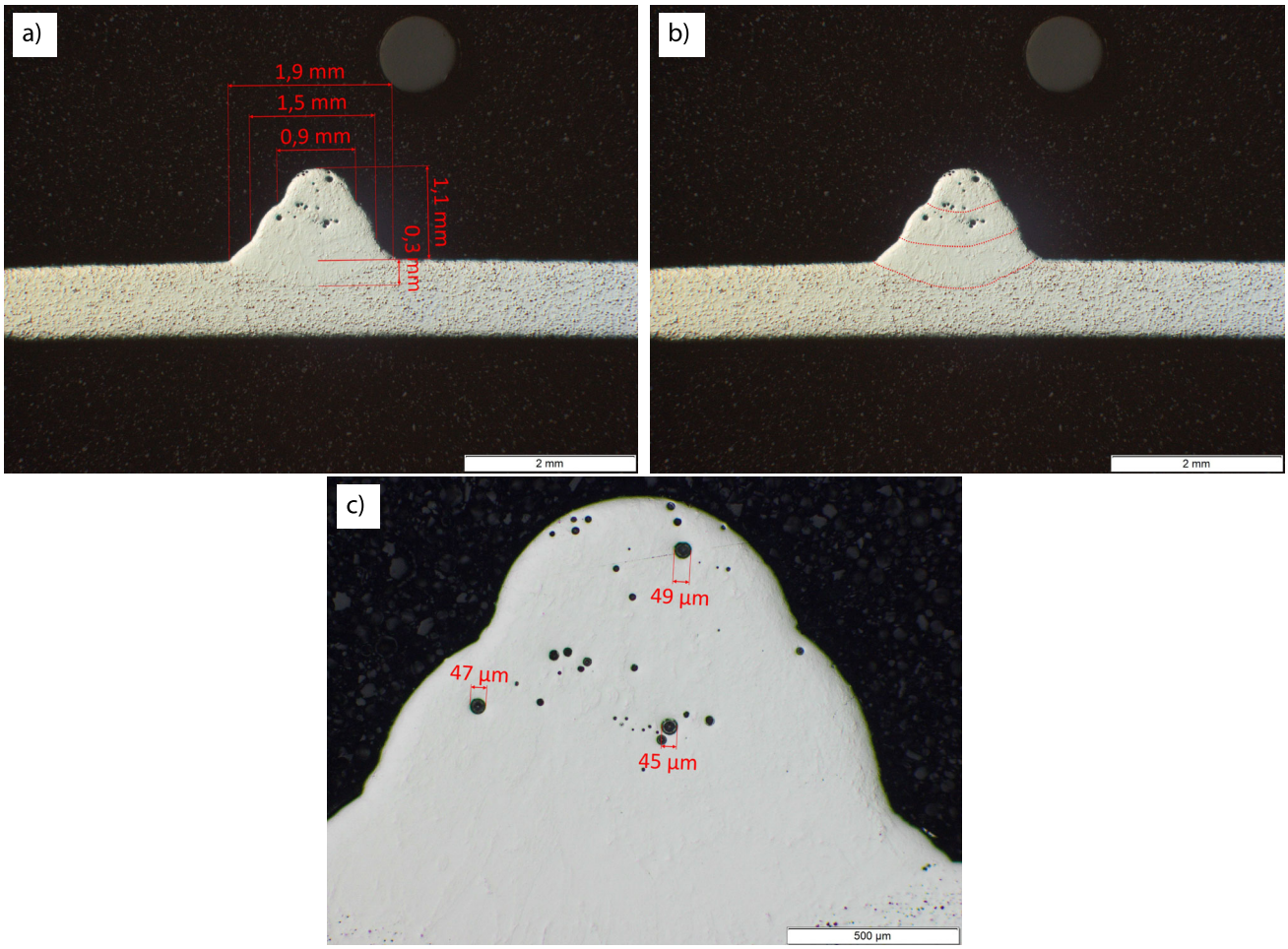

Fig. 6 Unetched LOM pictures of one exemplary pin including dimensions (**a**), depiction of the three layers (**b**) and magnification of the top part including measurement of maximum pore sizes (**c**)

Furthermore, to increase the robustness of the shear testing results, 10 individual pins were tested for each condition, ensuring meaningful average and standard deviation values.

2.5 Metallography and hardness testing

The metallographic specimens were precisely cut in the middle of the pins, carefully ground and polished for light optical microscopy. The micrographs were analyzed with an Olympus BX60 microscope in polished condition for macrostructure and porosity. To visualize the grain structure the Barker etchant was employed. Scanning electron microscopy was performed using a Tescan Mira 3 microscope at 20 kV in secondary electron (SE) and back-scattered electron (BSE) modes.

The hardness measurements were conducted on a Zwick/Roll DuraScan 70 G5 using HV 0.1 (100 g) with an indent time of 15 s.

3 Results

3.1 Light optical microscopy

3.1.1 Macrostructure

The pins possess a cone-like shape with an average base diameter of 1.9 mm and height of 1.1 mm. The solidus line during welding is approximately 0.3 mm below the plate surface (Fig. 6a). The deposition of the three individual droplets is visible in form of slight bulges on the outside of the cones (b).

The amount of porosity, due to trapped hydrogen, is quite low and restricted to the two top layers. The maximum pore size is below 50 µm, with the majority of pores ranging between 10 µm to 20 µm (c).

Very little to no variation or scatter was observed in the shape and size of the pins.

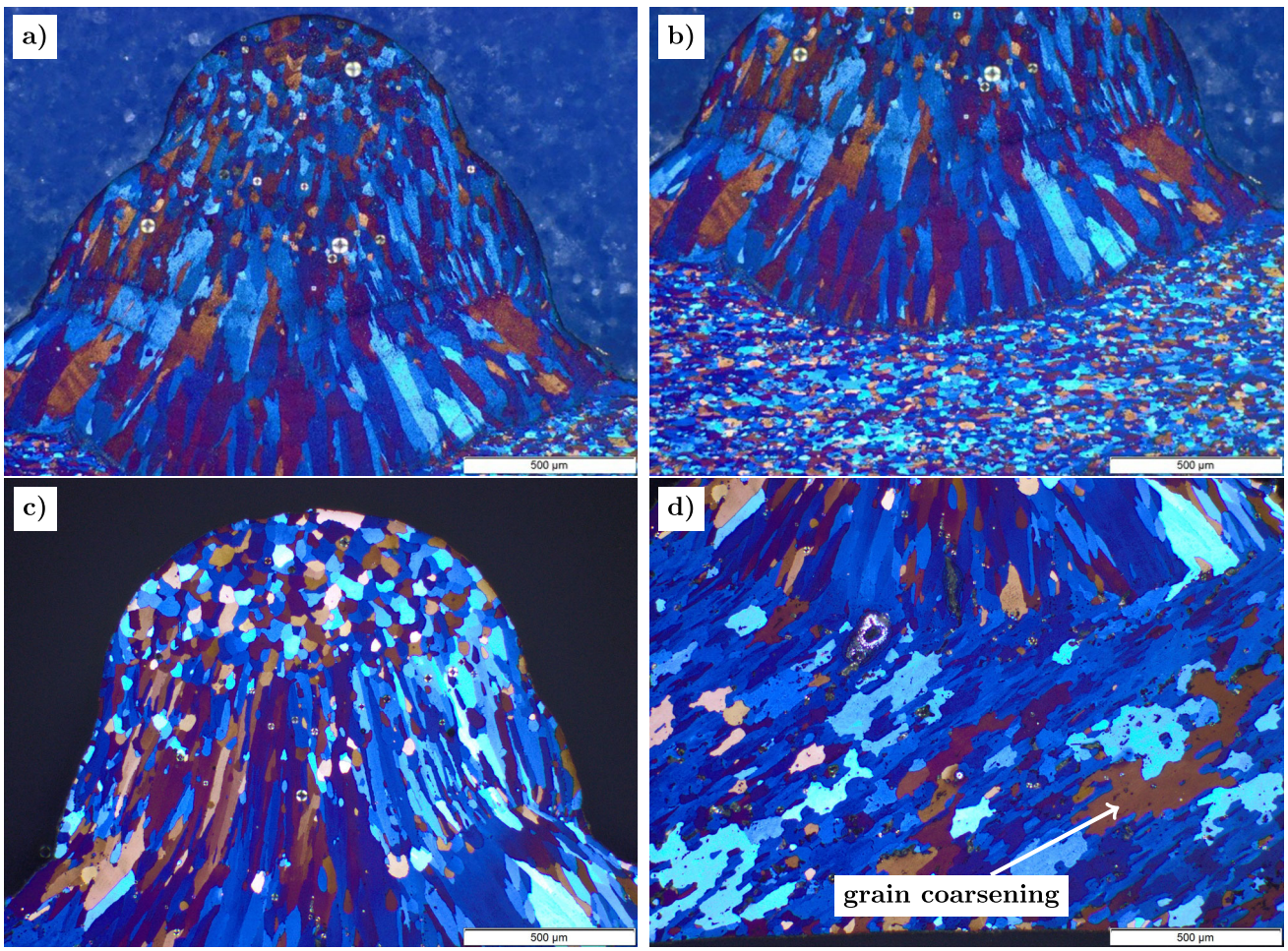

Fig. 7 Etched (Barker) LOM micrographs showing the microstructure of an exemplary pin in as-built (**a**,**b**) and T6 heat treated condition (**c**, **d**)

3.1.2 Microstructure

The etched cross-sections of the as-built condition (Fig. 7 a, b) reveal two very distinct microstructures in the pins. In the bottom droplet area columnar grains, orientated in the direction of the heat flow during *pinning*, are dominant. The grains grow across the layer boundary between droplets and can reach a maximum length of approximately 450 µm and maximum width of 60 µm.

In the second (middle) droplet area the columnar grain structure is continued, only the maximum grain size is slightly diminished. The columnar grain structure is also present in the lower part of the final droplet, however, at the top the microstructure changes to a more equiaxed composition. This so-called columnar-to-equiaxed transition (CET) is caused by the inhomogeneous temperature distribution within the weld pool. The development of different grain sizes and morphologies in weld metal can be described as a relationship between temperature gradient G (K m^{-1}) and growth velocity R (m s^{-1}) during solidification, see Fig. 8. On the one hand, the ratio G/R determines the grain morphology, high values result in planar and low values in equiaxed dendritic grain morphologies. On the other hand, the product GxR affects the grain size, whereat higher values yield finer structures [19–22].

In this case, in the base and middle drop a steep temperature gradient occurs, due to increased heat conduction into the "cold" base plate, resulting in a G/R ratio that supports columnar dendritic grain growth. During the deposition of the third drop the G/R ratio is lower, mainly because of a shallower T-gradient, and equiaxed grain growth is favored [21–23].

The T6 microstructure is comparable to the as-built condition (Fig. 7c, d). In the lower two droplets the grains are

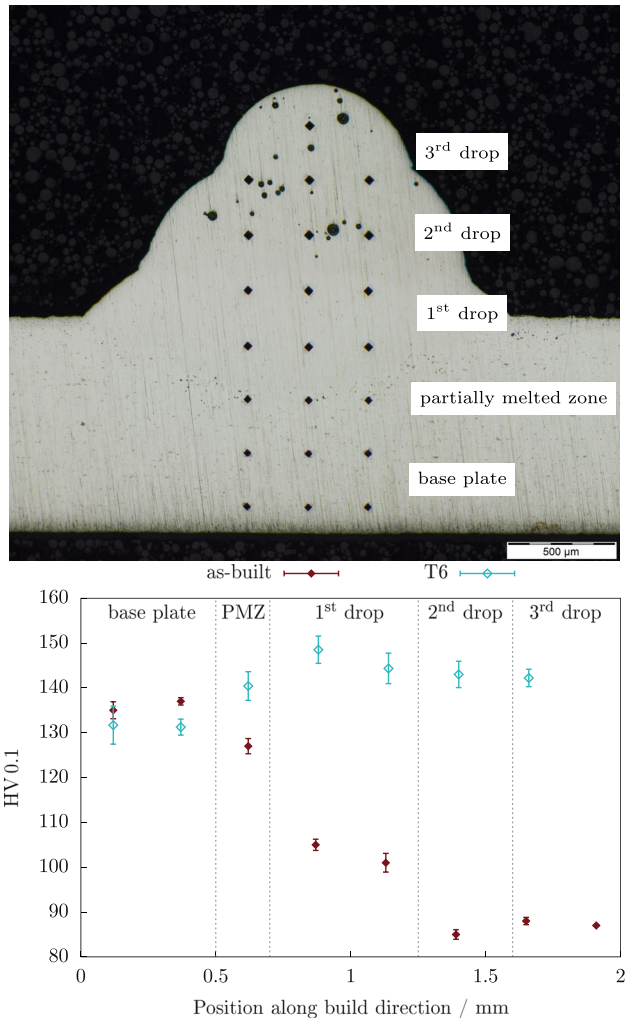

Fig. 9 Hardness Vickers indents (HV 0.1) across one aluminium pin (top) and corresponding hardness profiles (HV 0.1) in as-built (red) and T6 heat treated (turquoise) condition (bottom)

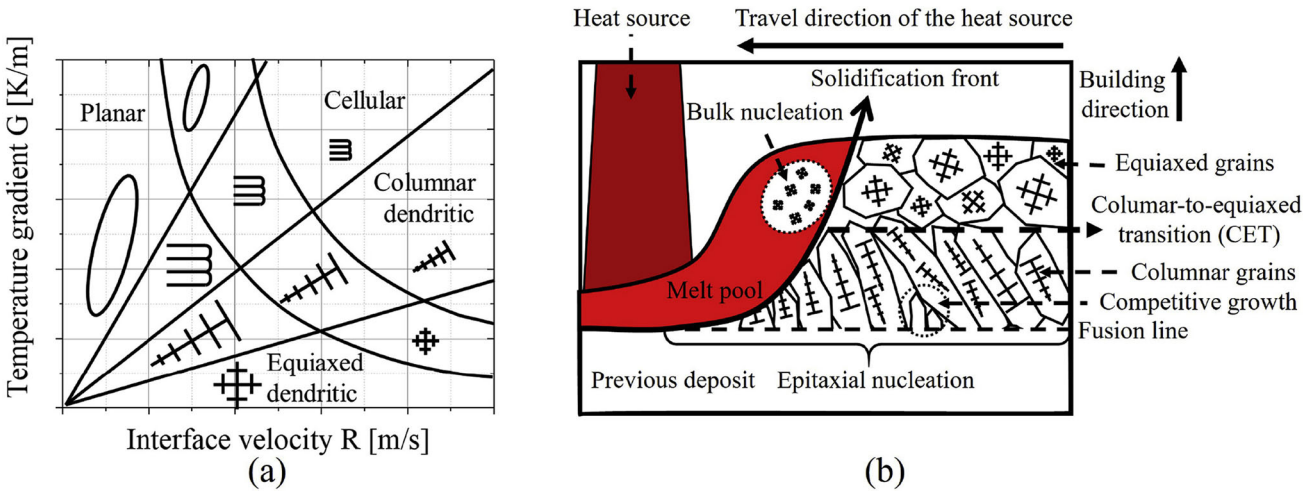

Fig. 8 The influence of interface velocity and temperature gradient on the development of grain morphology and grain size (**a**) and schematic representation of possible nucleation and growth mechanisms in the melt pool during metal deposition (**b**) [22]

columnar and grow across the layer boundary. The top droplet again exhibits an equiaxed grain structure. Distinct changes between the as-built and T6 condition can only be found in the base plate. The solution annealing results in visible grain coarsening (Fig. 7d, lower part).

3.1.3 Hardness

The microhardness profile of as-built pins (Fig. 9, red points) exhibits a decreasing hardness in build direction. The indents in the bottom two rows are still in the unaffected base material and show the highest hardness values in the range of 130 HV 0.1 to 140 HV 0.1. The next row of indents lies in the partially melted zone (PMZ) of the first droplet and the hardness slightly decreased to 127 HV 0.1. The hardness in the bottom droplet is on the one hand impaired by the coarse columnar grain structure and on the other hand elevated by the dilution between base material and filler material (higher strength level of the AW2024 base plate). An intermediate microhardness of 105 HV 0.1 was measured in this region. The fifth row of indents (from the bottom) lies in the heat affected zone between first and second droplets. Here, the hardness is only slightly reduced by the heat input to 101 HV 0.1. In the second droplet the lowest microhardness of 85 HV 0.1 was recorded. This can be explained by the combination of relatively coarse columnar grains and the missing dilution with the base material. The hardness level in the top droplet is similar to the second droplet, the small increase can be attributed to a smaller grainsize.

The T6 heat treatment reverses the hardness profile. The hardness increases in build direction. Interestingly, the base material shows a hardness level identical to the as-built condition. The hardening effect of the heat treatment is probably rescinded by the grain coarsening (see Fig. 7d). However, in T6 condition the microhardness of the pins is strongly increased, by 50 HV 0.1 to 60 HV 0.1, compared to the pins in as-built condition.

The porosity in the top region may affect the hardness values (in both temper conditions) due to changed material flow conditions. However, we believe the effect to be negligible since no scattering of the individual indent values was detected.

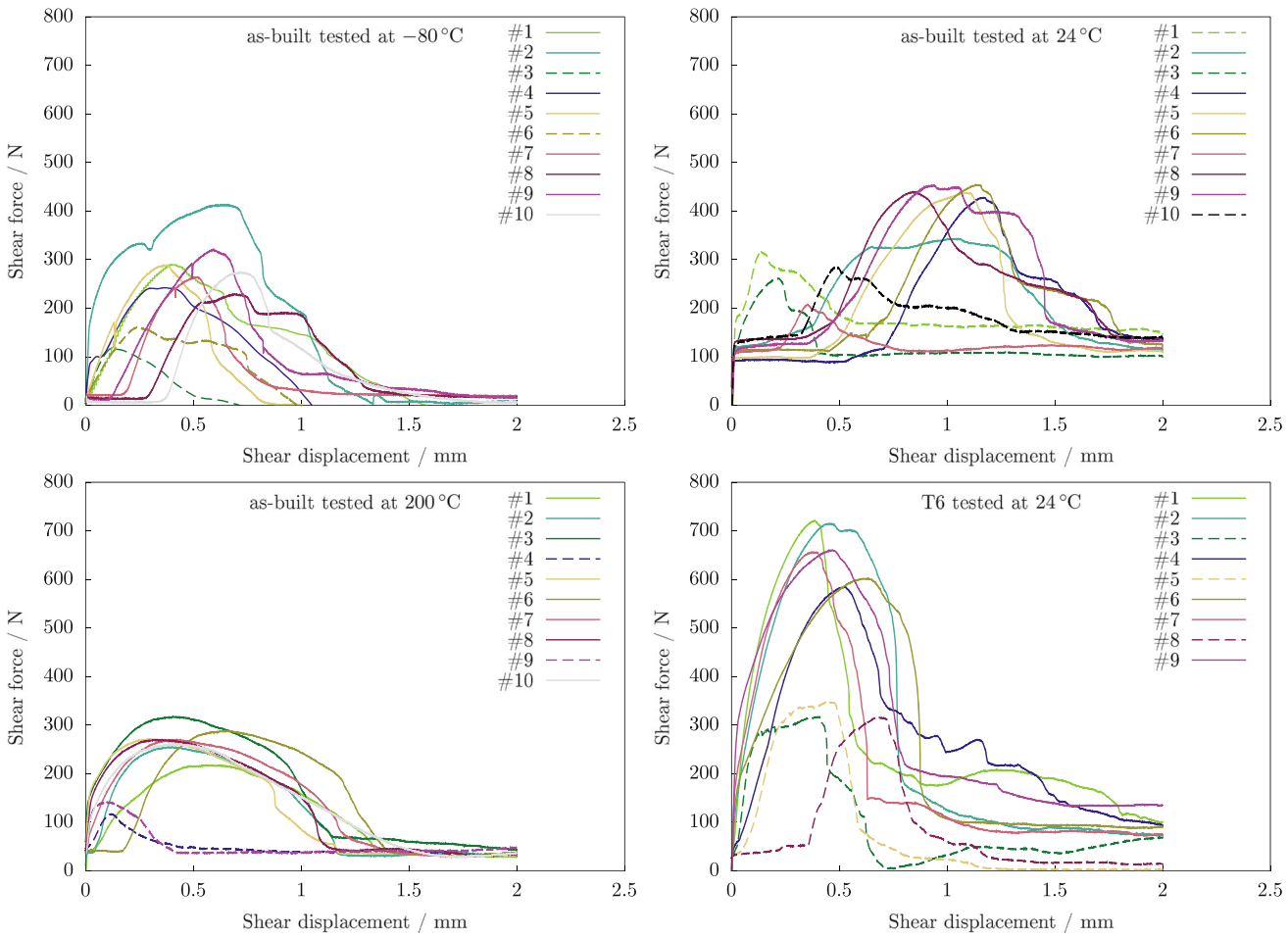

Fig. 10 Shear force-displacement curves of all tested single pins. The maximum displacement was limited to 2 mm

3.1.4 Shear testing

Shear testing of as-built pins was performed at -80°C, room temperature (RT, +24°C) and +200°C. Additionally, T6 heat treated samples were tested at RT.

As stated in the testing section, settling effects of the pins at the beginning of the measurements result in shifted force-displacement curves. This effect is especially pronounced for the pins tested at room temperature (Fig. 10, top right).

At -80°C and RT the shape of the force-displacement curves is similar for most of the tested pins. As soon as the pin is settled in the test apparatus the shear force steadily increases, reaches is maximum and rapidly decreases back to the starting point after the pin is sheared off. On average 25% of the pins exhibit a different behavior and much lower maximum shear forces were recorded. These outliers will be further discussed later on in the section about *Fracture surface analysis*.

The shape of the force-displacement curves changes at +200°C testing temperature. After the maximum shear force is reached, the force decreases only slightly as the pins deform plastically until fracture. The zone of plastic deformation is more pronounced compared to testing at -80°C or RT because of the enhanced ductility of the material at elevated temperature.

At room temperature the maximum average shear force was 382.5 MPa with a deviation of 24.9%. The values decreased to 259.6 MPa (29.9%) at -80°C and 240.8 MPa (25.3%) at +200°C test temperature. After T6 heat treatment the maximum average shear force increased by +42,6% to 547.0 MPa (29.4%) compared to the as-built condition (Fig. 11). The higher shear force values in T6 condition are consistent with the increased hardness levels shown in Fig. 9.

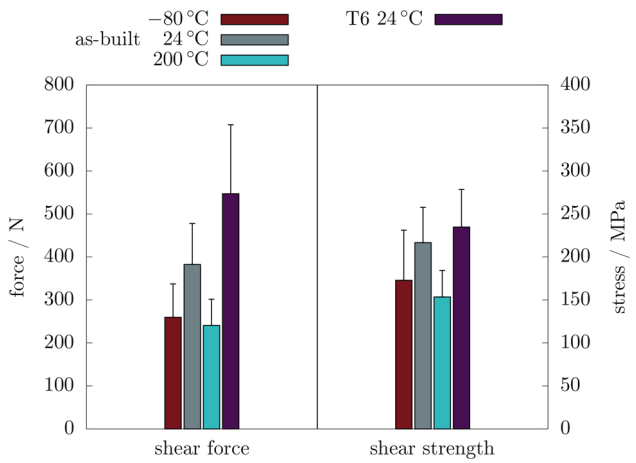

Fig. 11 Comparison of maximum average shear force and average shear strength at different testing temperatures and heat treatment conditions

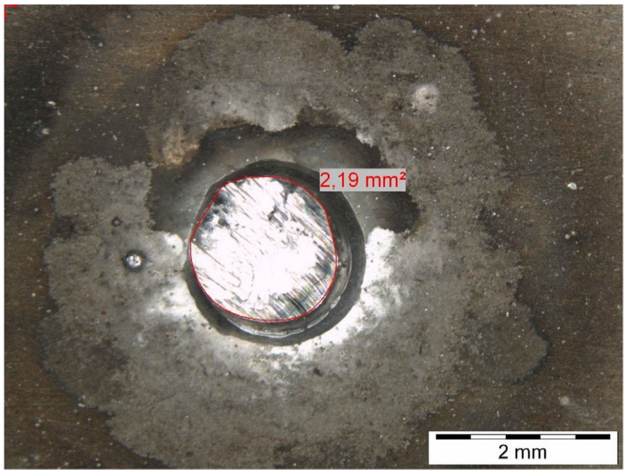

Fig. 12 Exemplary (sample #2) stereographic micrograph showing shear fracture surface and measured fracture area

In addition to the maximum shear force, the maximum shear stress was evaluated by measuring the fracture area of the tested pins (see Fig. 12). The average fracture area was 1.6 mm^2 for the pins tested at -80°C and +200°C. At RT the average fracture area increased to 1.8 mm^2 and in T6 condition to 2.3 mm^2. Due to the distinctly larger fracture area of the T6 pins, the maximum shear stress is only slightly higher compared to the as-built pins tested at room temperature (Fig. 11).

3.1.5 Fracture surface analysis

As already mentioned in the section about *Shear testing results*, 25% of the pins show a different failure behavior. Fracture surface analysis by means of scanning electron microscopy of corresponding pins revealed the underlying cause for these differences.

Pin #3 (maximum shear force 261 N) tested at room temperature, representing the outliers, exhibited a ragged and uneven fracture surface, with a multitude of visible pores and cracks (Fig. 13a). Most of the surface shows signs of ductile failure as revealed by the honeycomb structure (Fig. 13c). Only very little clear shear zones are observed. The pores act as a preferential cracking path, thus reducing the crack resistance.

Pin #5 (maximum shear force 438 N) tested at RT, exemplary for the standard failure mode, shows a completely different fracture surface. The surface is very smooth and only very few and small pores and cracks are visible. The smooth and shiny surface is a result of the two fracture surfaces being smeared together. This is consistent with dominant shear fracture mode [24, 25].

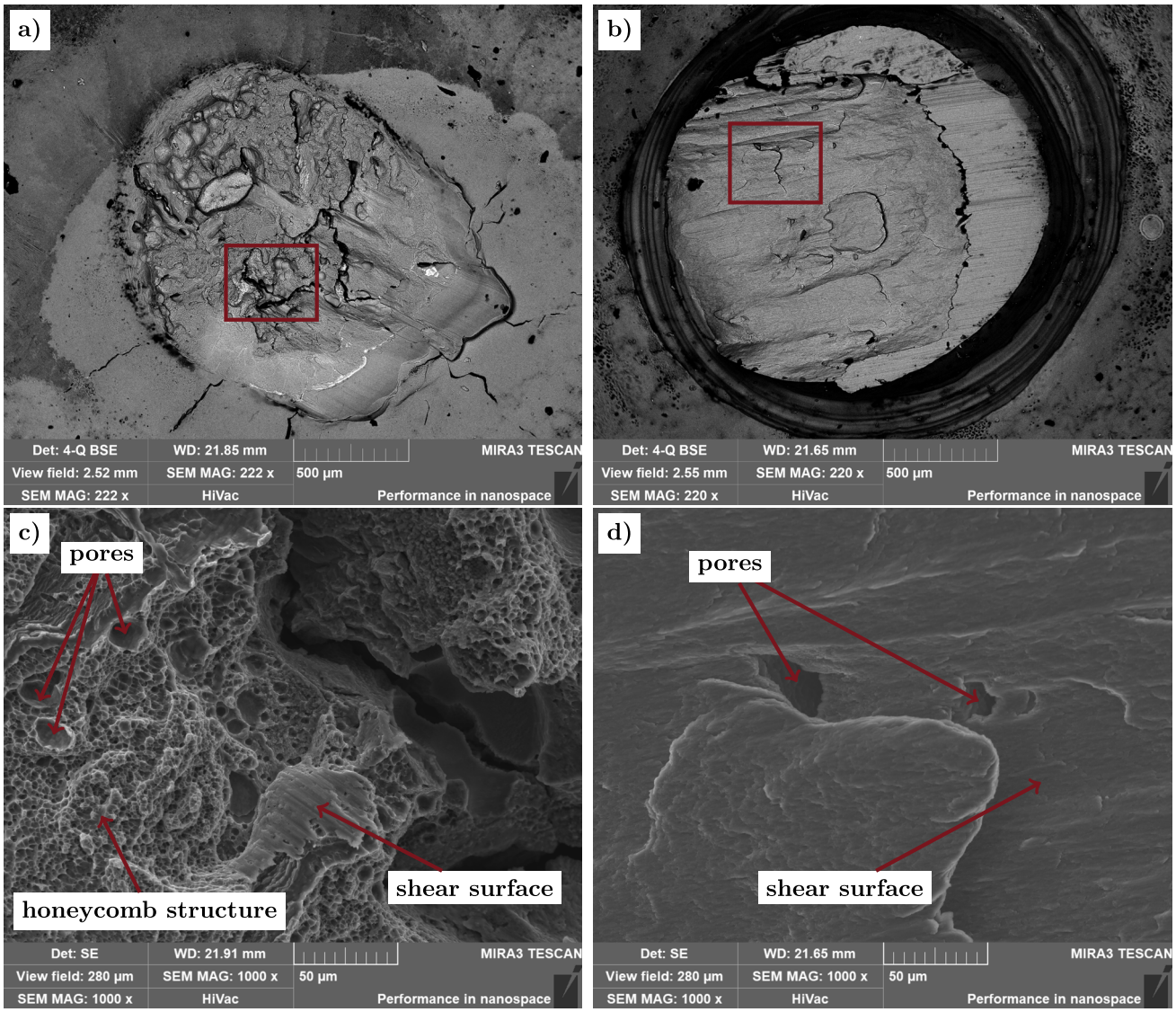

Fig. 13 Scanning electron micrographs (back-scattered electron mode, BSE) of the fracture surfaces of pin #3 (**a**) and pin #5 (**b**) tested at RT. The marked regions are shown in panels **c**) and **d**) at higher magnification and in secondary electron (SE) mode

4 Discussion

The macroscopic measurement of the S Al 2319 pins on AW2024 substrate sheets revealed almost no variation in shape and size of the individual pins. This was accomplished by precise parameter control during the modified CMT print process proving its robustness for continuous and high throughput pin production. The combination of low cycle time and high repeatability makes it suitable for a wide range of future applications [1, 6].

The amount of porosity was moderate and, in most cases, limited to the top two layers of the printed aluminium pins with a maximum height of 1.50 mm. In some instances, grouping of the pores along the boundary lines was observed which is consistent with literature on porosity in layered aluminium structures [26, 27]. The remelting allows the hydrogen to rise and cross over to the next layer. However, since the weld pool is very small and quickly solidifies, part of the hydrogen is trapped and forms pores upon solidification.

Although the degree of porosity is consistent for most investigated pins, sometimes the porosity was significantly higher in *poor* pins (Fig. 14). In these cases, pores were also observed in the bottom layer of the pins and the maximum pore diameter increased to 100 µm to 200 µm. The abnormal porosity did not coincide with changes in the pin shape or size, hinting towards an instability in the printing process. One reasonable explanation, which is also observed and discussed in other studies [28, 29], is varying quality of the welding wire. Especially residues, mostly lubricant from the

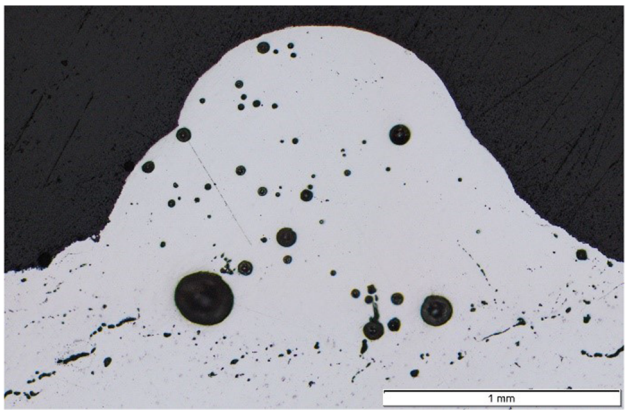

Fig. 14 Exemplary *poor* pin with significantly higher porosity, especially in the bottom layer

manufacturing process, are oftentimes found at the wire surface. These are trapped in grooves or scratches and remain there if not adequately cleaned. The amount of residues on the wire surface can vary strongly, even within one spool and strongly affects the quality of the welding process. A higher quality welding wire, with no unwanted inclusions or residues on its surface, would probably result in lower porosity hence higher quality pins.

In the top part of the pin the heat conduction is reduced by the smaller cross-section for heat flow, which results in a lower cooling rate. Consequently, the grains are more equiaxed and evenly distributed in this area. This change in microstructure is often observed in wire-arc-based direct energy deposition manufactured parts [30–32].

The subsequent application of T6 heat treatment did not affect the grain size of the pins. The as-built pin microstructure is undeformed and thus the driving force for recrystallization and grain coarsening during annealing is very low. The base material, however, was cold worked (T3 condition) prior to the welding and heat treatment process. Evidently the critical degree of deformation was exceeded, resulting in prominent grain coarsening during the annealing process (Fig. 7 bottom) [24, 33].

While the influence of the heat treatment is not visible in the etched grain structure of the pins, it becomes apparent in the hardness distribution. The T6 condition shows higher hardness values over the entire pin height compared to the as-built condition. This hardness increase is a direct result of the precipitation hardening during T6 tempering. In the base material the hardness does not vary between as-built and T6 condition. The strength increase due to T6 heat treatment was probably counteracted by the grain coarsening.

The pins are primarily designed to withstand shear forces during operation. To the authors knowledge no standardized test methods exist to test small pin-like structures in mode II loading conditions. Therefore, a new test method was designed and implemented for this study, as explained in Section 2.4 "Shear testing". Preliminary testing revealed difficulties with settling effects of the pins in the mount, which could be alleviated by preloading the pins with 10 N to 100 N.

As mentioned in Section 3, most of the force-displacement curves exhibit similar shapes for testing at -80°C and at room temperature. After settling of the pin in the test apparatus the shear force rapidly increases to its maximum and quickly drops as the pin is sheared off (Fig. 10). At 200°C testing temperature, however, the maximum average forces reduce significantly, and the zone of plastic deformation is much more pronounced, changing the overall shape of the force-displacement curves. This can be attributed to increased ductility as well as decreased yield strength of aluminium alloys at elevated temperatures as is well documented in the literature [34–37].

On average 25% of the samples, regardless of testing conditions, showed significant different behavior during shear testing. Fracture surface analysis using scanning electron microscopy revealed the underlying cause for these outliers. A higher number of pre-existing *welding* defects such as pores and cracks offer preferential cracking paths thus reducing the crack resistance and maximum recorded shear force, and ultimately results in reduced performance. The strong influence of weld quality in terms of porosity and cracks on the pin's shear resistance attests the need for an optimized welding process as well as wire feedstock. Overall weld quality depends on a multitude of factors but for porosity the main contributors are suitable process parameters and usage of high-quality welding wire [26, 28, 29, 38–40]. The adaption of process parameters is limited by the restricted processing window for pin fabrication further amplifying the necessity of high-quality welding wires.

5 Conclusions

The generation of novel small and *spiky* head aluminium pins with a nominal height of 1.50 mm was demonstrated in this work. In conjunction with the presented shear testing methodology it facilitates future application in ultra-lightweight CFRP-metal joints.

After comprehensive metallographic and mechanical characterization of the novel *spiky* head aluminium pins the following major conclusions can be drawn:

- A very robust pin printing process can be established by precise parameter control of the modified CMT print process. A low cycle time of approximately 150 ms enables fast and reliable pin fabrication.
- The quality of the welding wire plays an essential role in the properties of the pins, dominantly in terms of porosity. Distinct variation in the number and size of pores in the different pins was found.

- The presented adaption of the tensile test enables simple and effective shear testing (mode II) of metallic pins. This modification can be easily implemented in different tensile testing equipment, allowing more widespread usage. However, further improvements, such as locale displacement measurement and better clamping of individual pins, are needed to improve the robustness of the testing method.
- The new small and *spiky* head pins are able to withstand considerable shear forces, thanks to their wide base and proper welding connection with the base plate. The average shear force recorded at room temperature in as-built condition was 382.5 MPa and 547.0 MPa in peak aged condition, respectively. The T6 heat treatment results in increased shear resistance due to higher material strength.

6 Outlook

This study was limited to the metallographic and mechanic characterization of aluminium pins independent of their potential applications. In light of already shown applications, such as joint elements in ultra-lightweight aluminium-CFRP structures [6], further research on pin generation and modification improving the overall performance of components is ongoing. Commonly used strengthening fibers in CFRP (e.g. carbon fibers) are very brittle and easily damaged by the pins during the joining process. A reduction of fiber damage and better interlocking of the fibers with the pins could be achieved by further adapting the pin head geometry.

Author Contributions All authors contributed to the study conception and design. Material preparation, data collection and analysis were performed by Christian Schneider-Bröskamp, Martin Schnall, Alois Birgmann and Stephan Ucsnik. The first draft of the manuscript was written by Christian Schneider-Bröskamp and all authors commented on previous versions of the manuscript. All authors read and approved the final manuscript.

Funding Open access funding provided by AIT Austrian Institute of Technology GmbH. This work has been carried out in the framework of the ESA-TDE project ADALFIC *Advanced Aluminium Fittings in CFRP tubes* (CN 4000126211) and as part of project SUSTAINair funded under Grant-ID 101006952. The authors would like to thank in special the European Space Agency, ESA/ESTEC, TEC-MSS Structures Section; Structures, Mechanisms & Materials for valuable discussions as well as the project partners Sonaca S.A., as well as GMT Gummi-Metalltechnik for their valuable work and support of project ADALFIC.

Declarations

Competing interests The authors have no relevant financial or nonfinancial interests to disclose.

References

1. Ucsnik S, Scheerer M, Zaremba S, Pahr DH (2010) Experimental investigation of a novel hybrid metal-composite joining technology. Compos A Appl Sci Manuf 41(3):369–374. https://doi.org/10.1016/j.compositesa.2009.11.003
2. Ucsnik SA, Kirov G (2011) New possibility for the connection of metal sheets and fibre reinforced plastics. Mater Sci Forum 690:465–468. https://doi.org/10.4028/www.scientific.net/MSF.690.465
3. Parkes PN, Butler R, Meyer J, de Oliveira A (2014) Static strength of metal-composite joints with penetrative reinforcement. Compos Struct 118(1):250–256. https://doi.org/10.1016/j.compstruct.2014.07.019
4. Graham DP, Rezai A, Baker D, Smith PA, Watts JF (2014) The development and scalability of a high strength, damage tolerant, hybrid joining scheme for composite-metal structures. Compos A Appl Sci Manuf 64:11–24. https://doi.org/10.1016/j.compositesa.2014.04.018
5. Stelzer S, Ucsnik S, Pinter G (2016) Strength and damage tolerance of composite-composite joints with steel and titanium through the thickness reinforcements. Compos A Appl Sci Manuf 88:39–47. https://doi.org/10.1016/j.compositesa.2016.05.020
6. Ucsnik S, Schnall M, Birgmann A (2021) Load transfer behaviour of ultra-light-weight CFRP-metal struts under elevated and cryogenic working temperatures. In: Euromat, online
7. Kirth R, Ebel C (2012) Arrangement for connecting an elongate element to a further component. EP2162634
8. Stelzer S, Ucsnik S, Pinter G (2015) Fatigue behaviour of composite-composite joints reinforced with cold metal transfer welded pins. Int J Fatigue 81:37–47. https://doi.org/10.1016/j.ijfatigue.2015.06.004
9. Skhabovskyi I, Batista NL, Damato CA, Reis RP, Botelho EC, Scotti A (2017) Appraisal of fiber-metal laminate panels reinforced with metal pins deposited by CMT welding. Compos Struct 180:263–275. https://doi.org/10.1016/j.compstruct.2017.07.043
10. Seidlitz H, Fritzsche S, Ambrosio M, Kloshek A (2017) Advanced Welding Technology for Highly Stressable Multi-Material Designs with Fiber-Reinforced Plastics and Metals. Open J Compos Mater 07(03):166–177. https://doi.org/10.4236/ojcm.2017.73010
11. Shapovalov O, Ost L, Doynov N, Kuke F, Ambrosio M, Michailov V, Seidlitz H (2022) Substitution von metallischen Schubfeldern im Fahrzeugbau durch fügetechnische Integration von FKV-Schalen. In: DVS CONGRESS, Koblenz, pp 385–393
12. Wittwer L, Jank N, Bećirović A, Waldhör A, Enzinger N (2012) Influences on ARC Stability in Welding of Aluminum Pin-Structures. In: ICAA13 Pittsburgh, Springer International Publishing, Pittsburgh, USA, pp 795–800, https://doi.org/10.1007/978-3-319-48761-8_117

13. Somosköi G, Tötök I (2013) CMT Pin - Define the shape of the welded pin through welding parameters. Prod Process Syst 6(1):47–56
14. Reisgen U, Willms K, Schäfer J, Türker M, Hegger J, Classen M, Feldmann M, Kopp M (2019) Investigations on small-scaled welded structures of austenitic stainless steel. Kov Mater 57(6):397–405. https://doi.org/10.4149/km_2019_6_397
15. Zhang G, Zhao H, Xu X, Qiu G, Li Y, Lin Z (2019) Metallic bump assisted resistance spot welding (MBaRSW) of AA6061-T6 and bare DP590: Part I-printing of metallic bump. J Manuf Process 44:427–434. https://doi.org/10.1016/j.jmapro.2019.05.042
16. Bianchi F (2012) Numerical modelling of through-thickness reinforced structural joints. PhD Thesis, Cranfield University (June)
17. Reisgen U, Schiebahn A, Lotte J, Hopmann C, Schneider D, Neuhaus J (2020) Innovative joining technology for the production of hybrid components from FRP and metals. J Mater Process Technol 282:116674. https://doi.org/10.1016/j.jmatprotec.2020.116674
18. Fronius International GmbH (2013) CMT Process
19. Kurz W, Giovanola B, Trivedi R (1986) Theory of microstructural development during rapid solidification. Acta Metall 34(5):823–830. https://doi.org/10.1016/0001-6160(86)90056-8
20. Kou S (2003) Weld metal solidification ii: Microstructure within grains. Weld Metall 2:199–202
21. Li X, Tan W (2018) Numerical investigation of effects of nucleation mechanisms on grain structure in metal additive manufacturing. Comput Mater Sci 153:159–169. https://doi.org/10.1016/j.commatsci.2018.06.019
22. Froend M, Ventzke V, Dorn F, Kashaev N, Klusemann B, Enz J (2020) Microstructure by design: An approach of grain refinement and isotropy improvement in multi-layer wire-based laser metal deposition. Mater Sci Eng A 772:138635. https://doi.org/10.1016/j.msea.2019.138635
23. Yan F, Xiong W, Faierson EJ (2017) Grain structure control of additively manufactured metallic materials. Materials 10(11). https://doi.org/10.3390/ma10111260
24. ASM Handbook Committee (1991) Heat Treating of Aluminun Alloys. In: ASM Handbook: Heat Treating of Aluminium Alloy, pp 841–879. https://doi.org/10.1361/asmhba000
25. Pedersen KO, Børvik T, Hopperstad OS (2011) Fracture mechanisms of aluminium alloy AA7075-T651 under various loading conditions. Mater Des 32(1):97–107. https://doi.org/10.1016/j.matdes.2010.06.029
26. Gierth M, Henckell P, Ali Y, Scholl J, Bergmann JP (2020) Wire Arc Additive Manufacturing (WAAM) of aluminum alloy AlMg5Mn with energy-reduced Gas Metal Arc Welding (GMAW). Materials 13(12):1–22. https://doi.org/10.3390/ma13122671
27. Klein T, Schnall M, Gomes B, Warczok P, Fleischhacker D, Morais PJ (2021) Wire-arc additive manufacturing of a novel high-performance Al-Zn-Mg-Cu alloy: Processing, characterization and feasibility demonstration. Additive Manuf 37(July 2020):101663. https://doi.org/10.1016/j.addma.2020.101663
28. Gu JL, Ding JL, Cong BQ, Bai J, Gu HM, Williams SW, Zhai YC (2014) The Influence of Wire Properties on the Quality and Performance of Wire+Arc Additive Manufactured Aluminium Parts. Adv Mater Res 1081:210–214. https://doi.org/10.4028/www.scientific.net/amr.1081.210
29. Ryan EM, Sabin TJ, Watts JF, Whiting MJ (2018) The influence of build parameters and wire batch on porosity of wire and arc additive manufactured aluminium alloy 2319. J Mater Process Technol 262:577–584. https://doi.org/10.1016/j.jmatprotec.2018.07.030
30. Wang H, Jiang W, Ouyang J, Kovacevic R (2004) Rapid prototyping of 4043 Al-alloy parts by VP-GTAW. J Mater Process Technol 148(1):93–102. https://doi.org/10.1016/j.jmatprotec.2004.01.058
31. Wang L, Suo Y, Liang Z, Wang D, Wang Q (2019) Effect of titanium powder on microstructure and mechanical properties of wire + arc additively manufactured Al-Mg alloy. Mater Lett 241:231–234. https://doi.org/10.1016/j.matlet.2019.01.117
32. Klein T, Schnall M (2020) Control of macro-/microstructure and mechanical properties of a wire-arc additive manufactured aluminum alloy. Int J Adv Manuf Technol 108(1–2):235–244. https://doi.org/10.1007/s00170-020-05396-6
33. Kammer C (2002) Aluminium Taschenbuch Band 1 - Grundlagen und Werkstoffe, 16th edn. Beuth Verlag GmbH, Düsseldorf
34. Ayres RA (1979) Alloying aluminum with magnesium for ductility at warm temperatures (25 to 250°C). Metall Trans A 10(7):849–854. https://doi.org/10.1007/BF02658303
35. Painter M, Pearce R (1980) The elevated Temperature Behaviour of Some Al-Mg Alloys. Revue de metallurgie / Memoires et etudes scientifiques April:617–634
36. Skejić D, Ćurković I, Rukavina MJ (2017) Behaviour of aluminium structures in fire: A review. In: Applications of Structural Fire Engineering, Czech Technical University in Prague, Dubrovnik, Croatia, https://doi.org/10.14311/asfe.2015.047
37. Su MN, Young B (2019) Material properties of normal and high strength aluminium alloys at elevated temperatures. Thin-Walled Struct 137:463–471. https://doi.org/10.1016/j.tws.2019.01.012
38. Hauser T, Reisch RT, Breese PP, Lutz BS, Pantano M, Nalam Y, Bela K, Kamps T, Volpp J, Kaplan AF (2021) Porosity in wire arc additive manufacturing of aluminium alloys. Additive Manuf 41:101993. https://doi.org/10.1016/j.addma.2021.101993
39. Aldalur E, Suárez A, Veiga F (2021) Metal transfer modes for Wire Arc Additive Manufacturing Al-Mg alloys: Influence of heat input in microstructure and porosity. J Mater Process Technol 297:117271. https://doi.org/10.1016/j.jmatprotec.2021.117271
40. Fu R, Tang S, Lu J, Cui Y, Li Z, Zhang H, Xu T, Chen Z, Liu C (2021) Hot-wire arc additive manufacturing of aluminum alloy with reduced porosity and high deposition rate. Mater Des 199:109370. https://doi.org/10.1016/j.matdes.2020.109370